Polyoxo Alkoxide Clusters of Vanadium: Structural Characterization of the Decavanadate Core in the "Fully Reduced" Vanadium(IV) Species $[V_{10}O_{16}\{(OCH_2)_3CCH_2CH_3\}_4]^{4-}$ and $[V_{10}O_{14}(OH)_2\{(OCH_2)_3CCH_2OH\}_4]^{2-}$ and in the Mixed-Valence Clusters $[V^{IV}_8V^{V}_2O_{16}\{(OCH_2)_3CR\}_4]^{2-}$ (R = $-CH_2CH_3$, $-CH_3$)

M. Ishaque Khan,† Qin Chen,† D. P. Goshorn,‡ and Jon Zubieta*,†

Department of Chemistry, Syracuse University, Syracuse, New York 13244-4100, and Exxon Research and Engineering Company, Annandale, New Jersey 08801

Received July 28, 1992

The hydrothermal reaction of a mixture of vanadium oxides with $(HOCH_2)_3CCH_2OH$ in the presence of Me_3NHCl yields the reduced species $(Me_3NH)_2[V^{IV}_{10}O_{14}(OH)_2\{(OCH_2)CCH_2OH\}_4]\cdot 2H_2O$ (**1**). In contrast, the reactions of vanadium oxides with $(HOCH_2)_3CR$, using NaCl, KCl, or $(C_4H_9)_4NCl$ as mineralizers, yield the mixed-valence species $M_2[V^{IV}_8V^{V}_2O_{16}\{(OCH_2)_3CR\}_4]\cdot nH_2O$ (M = Na, n = 0, R = $-CH_2CH_3$ (**2**); M = K, n = 2, R = $-CH_2CH_3$ (**3**); M = $(C_4H_9)_4N$, n = 0, R = $-CH_3$ (**4**)). These compounds exhibit structures based on the decavanadate core $\{V_{10}O_{28}\}$, with ten doubly-bridging and two triply-bridging oxo groups of this parent structure replaced by the alkoxy donors of the ligands. The structural consequences of protonation of the core in **1** and of oxidation of two vanadium centers in **2**–**4** are presented. The crystal packing patterns of anion clusters and cations in these species reveal the common structural motif of anion stacking to produce polar and nonpolar channels. The influence of the cation on the details of the extended structure is apparent in the crystal packing descriptions. Crystal data are as follows. $(Me_3NH)_2[V_{10}O_{14}(OH)_2\{(OCH_2)_3CCH_2OH\}_4]\cdot 2H_2O$ (**1**): monoclinic space group $P2_1/c$, a = 10.243(2) Å, b = 18.237(4) Å, c = 13.055(2) Å, β = 103.48(2)°, V = 2371.5(9) Å^3, Z = 2, D_{calc} = 1.95 g cm^{-3}; structure solution and refinement based on 3505 reflections converged at R = 0.038. $Na_2[V_{10}O_{16}\{(OCH_2)_3CCH_2CH_3\}_4]$ (**2**): monoclinic space group $P2_1/c$, a = 12.861(2) Å, b = 10.536(2) Å, c = 15.909(4) Å, β = 109.21(2)°, V = 2035.7(8) Å^3, Z = 2, D_{calc} = 2.18 g cm^{-3}; 3006 reflections, R = 0.042. $K_2[V_{10}O_{16}\{(OCH_2)_3CCH_2CH_3\}_4]\cdot 2H_2O$ (**3**): triclinic space group $P\bar{1}$, a = 10.249(2) Å, b = 12.438(2) Å, c = 9.903(2) Å, α = 97.51(1)°, β = 109.30(1)°, γ = 68.41(1)°, V = 1107.8(6) Å^3, D_{calc} = 2.10 g cm^{-3}; 4441 reflections, R = 0.030. $[(C_4H_9)_4N]_2[V_{10}O_{16}\{(OCH_2)_3CCH_3\}_4]$ (**4**): monoclinic space group, $P2_1/n$, a = 13.523(4) Å, b = 18.453(3) Å, c = 14.375(6) Å, β = 104.87(2)°, V = 3466.9(15) Å^3, Z = 2, D_{calc} = 1.65 g cm^{-3}; 2964 reflections, R = 0.047.

Recent investigations of the coordination chemistry of isopolymetalates[1,2] with organic ligands have revealed an extensive class of polyoxo alkoxide clusters.[3-10] The use of multidentate alkoxy ligand types has allowed the preparation of a variety of unusual polyoxomolybdate structural types, including the trinuclear complex $[Mo_3O_7\{(OCH_2)_3CR\}_2]^{2-}$, which represents a unique example of a solution stable cluster containing the facial terminal trioxomolybdate(VI) unit.[5] Extensions of these investigations to the polyoxovanadium class of clusters has allowed the development both of novel structural types and of cores containing reduced metal centers, rather than the more common "oxidized" clusters which exhibit all metal centers in the nd^0 configuration.

In the course of our investigations of this emerging structural class of alkoxopolyoxometalate oligomers, we have described a series of hexavanadium clusters of nearly identical structure but with different electron populations and protonation sites, as well as different types of spin–spin interactions, namely, $[V_6O_{13-n}(OH)_n\{(OCH_2)_3CR\}_2]^{2-}$ with n = 2, 4, and 6.[9,10] Furthermore, by employing the techniques of hydrothermal synthesis, we have demonstrated that sequential substitution of bridging oxo groups by alkoxide ligands allows the preparation of a family of alkoxopolyoxovanadium clusters with the hexavanadate core, $[V_6O_{19-3n}\{(OCH_2)_3CR\}_n]^{x-}$ (n = 2–4).[11]

Since the products of the hydrothermal reactions were sensitive both to reaction times and temperatures and to the identity of the cations introduced, the influences of variable reaction conditions on product composition were studied in detail. Under appropriate conditions, larger aggregates were observed to form, and several examples of reduced polyoxoalkoxovanadium clusters based on the decavanadate core $[V_{10}O_{28}]^{6-}$ (A) were isolated.[12,13] These clusters, of general composition $[V_{10}O_{28-3n}\{(OCH_2)_3CR\}_n]^{x-}$ (n = 4, x = 4; n = 5, x = 1), are related to the parent core through substitution of sets of doubly and triply bridging oxo groups, located on the triangular cavities formed by the fusion of three $\{VO_6\}$ octahedra, by the oxygen donors of the trisalkoxide ligand. Further exploitation of the hydrothermal technique revealed that

† Syracuse University.
‡ Exxon.

(1) Pope, M. T.; Müller, A. *Angew. Chem., Int. Ed. Engl.* **1991**, *30*, 34. Pope, M. T. In *Comprehensive Coordination Chemistry*; Wilkinson, G., Gillard, R. D., McCleverty, J. A., Eds.; Pergamon: Oxford, England, 1987; Vol. 3, p 1023. Pope, M. T. *Heteropoly and Isopoly Oxometalates*; Springer: New York, 1983.
(2) Day, V. W.; Klemperer, W. G. *Science* (*Washington, D.C.*) **1985**, *228*, 533.
(3) Chen, Q.; Zubieta, J. *Coord. Chem. Rev.* **1992**, 0000.
(4) Ma, L.; Liu, S.; Zubieta, J. *J. Chem. Soc., Chem. Commun.* **1989**, 440.
(5) Ma, L.; Liu, S.; Zubieta, J. *Inorg. Chem.* **1989**, *28*, 175.
(6) Liu, S.; Ma, L.; McGowty, D.; Zubieta, J. *Polyhedron* **1990**, *9*, 1541.
(7) Chen, Q.; Liu, S.; Zubieta, J. *Inorg. Chem.* **1989**, *28*, 4433.
(8) Chen, Q.; Liu, S.; Zubieta, J. *Angew. Chem., Int. Ed. Engl.* **1990**, *29*, 70.
(9) Chen, Q.; Zubieta, J. *Inorg. Chem.* **1990**, *29*, 1458.
(10) Chen, Q.; Goshorn, D.; Scholes, C.; Tan, X.; Zubieta, J. *J. Am. Chem. Soc.* **1992**, *114*, 4667.
(11) Khan, M. I.; Chen, Q.; Zubieta, J.; Goshorn, D. P. *Inorg. Chem.* **1992**, *31*, 1556.
(12) Khan, M. I.; Chen, Q.; Zubieta, J. *J. Chem. Soc., Chem. Commun.* **1992**, 305.
(13) Khan, M. I.; Chen, Q.; Goshorn, D. P.; Hope, H.; Parkin, S.; Zubieta, J. *J. Am. Chem. Soc.* **1992**, *114*, 3341.

0020-1669/93/1332-0672$04.00/0

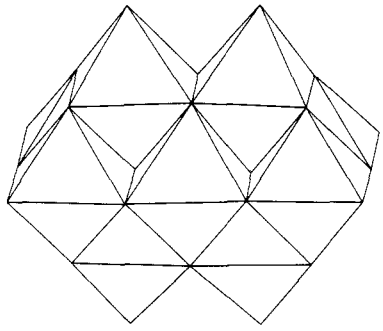

A

clusters with nearly identical core structures but displaying different oxidation states or protonation patterns could also be isolated. In this paper, we describe the synthesis and structures of four new decavanadium clusters $(Me_3NH)_2[V^{IV}_{10}O_{14}(OH)_2\{(OCH_2)_3CCH_2OH\}_4]\cdot 2H_2O$ (**1**), $Na_2[V^{IV}_8V^{V}_2O_{16}\{(OCH_2)_3CCH_2CH_3\}_4]$ (**2**), $K_2[V^{IV}_8V^{V}_2O_{16}\{(OCH_2)_3CCH_2CH_3\}_4]\cdot 2H_2O$ (**3**), and $(TBA)_2[V^{IV}_8V^{V}_2O_{16}\{(OCH_2)_3CCH_3\}_4]$ (**4**) (TBA = $(n\text{-}C_4H_9)_4N$) and discuss their structures in relation to the previously reported $(NH_4)_4[V^{IV}_{10}O_{16}\{(OCH_2)_3CCH_2CH_3\}_4]\cdot 4H_2O$ (**5**) and $[(C_2H_5)_4N][V_{10}O_{13}\{(OCH_2)_3CCH_2CH_3\}_5]$ (**6**).[13]

Experimental Section

Reagent grade chemicals were used throughout. Vanadium(III) oxide (Aldrich), vanadium(V) oxide (Aldrich), sodium metavanadate (Alfa), 1,1,1-tris(hydroxymethyl)alkanes (Fluka), pentaerythritol (Aldrich), trimethylammonium hydrochloride (Aldrich), and potassium chloride (Alfa) were used as received from the commercial sources. All reactions were carried out in 23-mL Parr Teflon-lined acid digestion bombs, heated in a Thermolyne programmable electric furnace. While preparations using each of the ligand types $RC(CH_2OH)_3$ (R = CH_3–, CH_3CH_2–, $HOCH_2$–) were attempted for all sets of conditions, synthetic details are given only for those instances which produced crystalline materials in appreciable yield.

Preparation of $(Me_3NH)_2[V_{10}O_{14}(OH)_2\{(OCH_2)_3CCH_2OH\}_4]\cdot 2H_2O$ (1). Vanadium(III) oxide, vanadium(V) oxide, sodium metavanadate, pentaerythritol, trimethylamine hydrochloride, and water in the molar ratio 5:5:5:10:20:300 were placed in a Parr Teflon-lined acid digestion bomb of 23-mL capacity, which was subsequently heated for 20 h in a Thermolyne electric furnace maintained at 150 °C. After cooling of the reaction bomb to room temperature, dark gray-black crystals of **1** were filtered out, washed carefully with water, and air dried (yield: 40% based on vanadium). Anal. Calcd for $C_{26}H_{62}N_2O_{34}V_{10}$: C, 21.4; H, 4.26; N, 1.92. Found: C, 21.8; H, 4.23; N, 2.11. IR (KBr pellet, cm^{-1}): 1475 (m), 1454 (m), 1114 (vs), 1061 (s), 1019 (vs), 974 (vs), 838 (s), 645 (s), 592 (s), 557 (w).

Preparation of $Na_2[V_{10}O_{16}\{(OCH_2)_3CCH_2CH_3\}_4]$ (2). A mixture of vanadium(III) oxide, sodium metavanadate, sodium chloride, copper(I) bromide, 1,1,1-tris(hydroxymethyl)propane, and water in the molar ratio 3:6:5:10:10:300 was placed in a Parr Teflon-lined acid digestion bomb and heated for 50 h at 150 °C in a Thermolyne electric furnace. The resulting mixture was allowed to cool to room temperture, whereupon dark brown crystals of **2** and a small amount of shiny blue crystals of $Na_2[V_6O_7\{(OCH_2)_3CCH_2CH_3\}_4]$ were collected by filtration. After washing with water and drying, crystals of **2** were separated from the hexavanadium byproduct by hand under the microscope. (Yield: 35% based on vanadium.) Anal. Calcd for $C_{24}H_{44}O_{28}Na_2V_{10}$: C, 21.6; H, 3.29. Found: C, 22.1; H, 3.52. IR (KBr pellet, cm^{-1}): 1467 (m), 1447 (m), 1200 (m), 1112 (s), 1042 (vs), 998 (s), 987 (vs), 977 (vs), 964 (vs), 940 (s), 847 (s), 775 (m), 617 (vs), 600 (s), 583 (s), 564 (s), 537 (m), 424 (m). While CuBr does not appear in the product, its use is crucial to obtaining reasonable yields of **2**. In the absence of CuBr, yields on the order of 5% are obtained. CuCl may be substituted for CuBr.

Preparation of $K_2[V_{10}O_{16}\{(OCH_2)_3CCH_2CH_3\}_4]\cdot 2H_2O$ (3). Vanadium(III) oxide, potassium metavanadate, potassium chloride, manganese(II) chloride, 1,1,1-tris(hydroxymethyl)propane, and water in molar ratio 3:6:10:10:10:300 were placed in a Parr Teflon-lined acid digestion bomb of 23-mL volume. After heating of this reaction mixture for 40 h at 150 °C in an electric furnace, it was cooled to ambient temperature. Dark brownish-gray colored crystals of **3**, along with some blue needlelike crystaline impurity tentatively identified as $K_2[V_6O_7\{(OCH_2)_3CCH_2CH_3\}_4]$, were filtered from the mother liquor, washed with water, and air dried. Crystals of **3** were mechanically separated from the byproduct under the microscope. (Yield: 25% based on vanadium.) Anal. Calcd for $C_{24}H_{48}O_{30}K_2V_{10}$: C, 20.5; H, 3.42. Found: C, 20.2; H, 3.37. IR (KBr pellet cm^{-1}): 1468 (m), 1445 (m), 1200 (m), 1115 (s), 1042 (vs), 995 (s), 979 (vs), 970 (vs), 961 (vs), 943 (s), 850 (s), 780 (m), 768 (w), 616 (vs), 590, 573 (vs), 545 (w), 531 (w), 480 (m). Again, the use of $MnCl_2$ was found to be required in order to obtain useful yields of crystalline materials.

Preparation of $[(C_4H_9)_4N]_2[V_{10}O_{16}\{(OCH_2)_3CCH_3\}_4$ (4). A Teflon-lined Parr acid digestion bomb, charged with vanadium(III) oxide, vanadium(V) oxide, vanadyl sulfate hydrate, 1,1,1-tris(hydroxymethyl)-ethane, tetrabutylammonium hydroxide (40 wt % solution in water), and water in the molar ratio 3:3:6:10:10:110 was heated for 90 h in an electric furnace maintained at 150 °C. After cooling of the reaction vessel at room temperature for 2 h, the solid reaction product was filtered from the light greenish-blue mother liquor and washed with copious amounts of water. Dark black crystal of **4** were separated by decantation and air dried (yield: 45% based on vanadium). Anal. Calcd for $C_{52}H_{108}N_2O_{28}V_{10}$: C, 36.3; H, 6.29; N, 1.63. Found: C, 35.8; H, 6.01; N, 1.54. IR (KBr pellet, cm^{-1}): 1480 (m), 1457 (m), 1128 (s), 1043 (vs), 983 (sh), 970 (vs), 838 (s), 780 (m), 575 (vs), 475 (m).

X-ray Crystallographic Studies. Compounds **1–4** were studied using a Rigaku AFC5S diffractometer. The crystal parameters and experimental conditions of the data collections are summarized in Table I. A complete description of the crystallographic methods is given in the supplementary material. The X-ray study of **4** was performed at –30 °C due to crystal instability in the X-ray beam at room temperature. No significant decomposition occurred at –30 °C over the time of this data collection.

The structures were solved by direct methods and refined by full-matrix least squares. The details of the structure solutions and refinements are presented in the supplementary material. No anomalies were encountered in the refinements of the structures. In the case of structure **1**, the hydrogen positions were located directly from the difference Fourier maps. After full-matrix least-squares refinement cycles using anisotropic thermal parameters for all non-hydrogen atoms of the anion, the cation, and the water molecule of crystallization, and fixed isotropic temperature factors for the hydrogen atoms associated with ligand and cation carbon centers (positioned at idealized C–H distances of 0.96 Å), the difference Fourier synthesis revealed electron density maxima consistent with protonation of O10, with the hydrogen atoms associated with the oxygen O17 of the water molecule, and with the hydrogen atom of the trialkylammonium cation. The locations of the hydrogen atoms were confirmed by high-angle ($2\theta > 37°$) refinement of the non-hydrogen atoms followed by difference Fourier synthesis based on inner shell data. This procedure clearly revealed all but the hydrogens associated with the pendant and disordered hydroxyl groups of the ligands. The hydrogens associated with O10, O17, and the nitrogen of the cation were included in the structural model and refined as independent isotropic atoms in the final least-squares cycle.

As noted above, the pendant –O(H) group of the ligand is disordered. The disorder was modeled as two half-occupancy sites for each of the crystallographically independent pendant oxygen atoms O16/O16a and O17/O17a.

For structures **2–4**, hydrogen atoms were included in the structure factor calculation at their calculated positions but were not refined. Selected bond lengths and angles for **1–4** are given in Table IV. Atomic positional parameters and temperature factors for all structures have been deposited as supplementary material.

Magnetic Susceptibility Studies. Magnetic susceptibility data for powdered samples of the compounds were obtained over a temperature range 5–300 K in an applied field of 6 G using a Quantum Design Model MPMS SQUID magnetometer. Magnetization isotherms at 298 and 77 K were performed to correct for the presence of ferromagnetic impurities.

Results and Discussion

General Properties. Despite a long history of application to geochemistry and to synthetic crystal growth,[14] the techniques of hydrothermal synthesis have only recently been exploited in

(14) Laudise, R. A. *Sci. Eng. News* **1987**, Sept 28, 30.

Table I. Summary of Crystal Data and Experimental Parameters for the X-ray Crystallographic Studies of $(Me_3NH)_2[V_{10}O_{14}(OH)_2\{(OCH_2)_3CCH_2OH\}_4]\cdot 2H_2O$ (**1**), $Na_2[V_{10}O_{16}\{(OCH_2)_3CCH_2CH_3\}_4]$ (**2**), $K_2[V_{10}O_{16}\{(OCH_2)_3CCH_2CH_3\}_4]\cdot 2H_2O$ (**3**), and $[(C_4H_9)_4N]_2[V_{10}O_{16}\{(OCH_2)_3CCH_3\}_4]$ (**4**)

	1	**2**	**3**	**4**
chem formula	$C_{26}H_{62}N_2O_{34}V_{10}$	$C_{24}H_{44}O_{28}Na_2V_{10}$	$C_{24}H_{48}O_{30}K_2V_{10}$	$C_{52}H_{108}N_2O_{28}V_{10}$
a, Å	10.243(2)	12.861(2)	10.249(2)	13.523(4)
b, Å	18.237(4)	10.536(2)	12.438(2)	18.453(3)
c, Å	13.055(2)	15.909(4)	9.903(2)	14.375(6)
α, deg	90.00	90.00	97.51(1)	90.00
β, deg	103.48(2)	109.21(2)	109.30(1)	104.87(2)
γ, deg	90.00	90.00	68.41(1)	90.00
Å^3	2371.5(9)	2035.7(8)	1107.8(6)	3466.9(15)
Z	2	2	1	2
fw	1456.0	1336.0	1404.2	1718.8
space group	$P2_1/c$ (No. 14)	$P2_1/c$ (No. 14)	$P\bar{1}$ (No. 2)	$P2_1/n$ (No. 14)
T, °C	22	22	22	−30
λ, Å	0.710 73	0.710 73	0.710 73	0.710 73
D_{calc}, g cm^{-3}	2.03	2.18	2.10	1.65
μ, cm^{-1}	19.17	22.31	22.91	13.19
R^a	0.038	0.042	0.030	0.047
$R_w{}^b$	0.050	0.044	0.033	0.053
GOF	2.07	1.18	1.11	1.72

^{a} $R = \sum||F_o| - |F_c||/\sum|F_o|$. ^{b} $R_w = \{[\sum w(F_o - F_c)^2]/[\sum w(F_o)^2]\}^{1/2}$.

Table II. Comparison of the 700–1000-cm^{-1} Range of the Infrared Spectra of Clusters with the $\{V_6O_{19}\}$ and $\{V_{10}O_{28}\}$ Cores

complex	ν(V–O$_t$)	ν(V–O–V)	ref
$(TBA)_2[V^V{}_6O_{13}\{(OCH_2)_3CNO_2\}_2]$	960, 944	800, 719	10
$(TBA)_2[V^V{}_6O_{13}\{(OCH_2)_3CCH_2OH\}_2]$	950	810, 715	10
$(TBA)_2[V^V{}_6O_{13}\{(OCH_2)_3CCH_3\}_2]$	960, 940	816, 710	10
$(TBA)_2[V^V{}_6O_{13}\{(OCH_2)_3CNHC(O)CHCH_2\}_2]$	956	809, 723	10
$(C_5H_5NH)_2[V^V{}_6O_{13}\{(OCH_2)_3CCH_3\}_2]$	958	789, 704	10
$[V^V{}_6O_{11}(OH)_2\{(OCH_2)_3CCH_3\}_2]$	954	796, 711	10
$Na_2[V^V{}_6O_7\{(OCH_2)_3CCH_2CH_3\}_4]$	950	*a*	11
$(Me_3NH)[V^{IV}{}_5V^VO_7(OH)_3\{(OCH_2)CCH_3\}_3]$	978, 949	726	11
$(NR_4)_3[H_3V^V{}_{10}O_{28}]$	968, 940	840, 803, 770	19, 20, 23^b
$(NR_4)_6[V^V{}_{10}O_{28}]$	965, 950, 931	887, 815, 750	19, 20^b
$(NH_4)_4[V^{IV}{}_{10}O_{16}\{(OCH_2)_3CCH_2CH_3\}_4]$ (**5**)	972, 942	840, 773	12, 13
$(Et_4N)[V^{IV}{}_{10}O_{13}\{(OCH_2)_3CCH_2CH_3\}_5]$ (**6**)	979, 941	836, 778	12, 12
$(Me_3NH)_2[V^{IV}{}_{10}O_{14}(OH)_2\{(OCH_2)_3CCH_2OH\}_4]$ (**1**)	974	838	this work
$Na_2[V^{IV}{}_8V^V{}_2O_{16}\{(OCH_2)_3CCH_2CH_3\}_4]$ (**2**)	998, 987, 977, 964, 940	847, 775	this work
$K_2[V^{IV}{}_8V^V{}_2O_{16}\{(OCH_2)_3CCH_2CH_3\}_4]\cdot 2H_2O$ (**3**)	995, 979, 970, 961, 943	850, 780	this work
$(TBA)_2[V^{IV}{}_8V^V{}_2O_{16}\{(OCH_2)_3CCH_3\}_4]$ (**4**)	983, 970, 950	838, 780	this work

^{a} No doubly bridging oxo groups are present in the structure of $Na_2[V_6O_7\{(OCH_2)_3CCH_2CH_3\}_4]$. ^{b} Published reports of the infrared spectra of $[V_{10}O_{28}]^{6-}$ and $[H_3V_{10}O_{28}]^{3-}$ are not in agreement. Our samples of $(TBA)_3[H_3V_{10}O_{28}]$ and $(TBA)_6[V_{10}O_{28}]$ are in close agreement with those published in refs 23 and 19, respectively.

the routine preparation of inorganic materials,[15] most prominently in the synthesis of polyoxomolybdenum- and polyoxovanadium–phosphorus species with reduced metal centers[16,17] and of materials of the vanadium/phosphate system.[18]

The reaction of V_2O_5, V_2O_3, $NaVO_3$, pentaerythritol, Me_3NHCl, and water in the mole ratio 5:5:5:10:20:300 under hydrothermal conditions yielded lustrous black crystals of $(Me_3NH)_2[V_{10}O_{14}(OH)_2\{(OCH_2)_3CCH_2OH\}_4]\cdot 2H_2O$ (**1**). The infrared spectrum of **1** exhibited the characteristic ligand ν(C–O) band at 1019 cm^{-1}, a strong absorption at 974 cm^{-1} associated with ν(V–O$_t$), and a medium-intensity feature at 838 cm^{-1} attributed to ν(V–O–V). In contrast, the reaction of V_2O_3, $NaVO_3$, NaCl, CuBr, 1,1,1-tris(hydroxymethyl)propane, and water in the mole ratio 3:6:5:10:10:300 produced dark brown crystals of the mixed-valence cluster $Na_2[V^{IV}{}_8V^V{}_2O_{16}\{(OCH_2)_3CCH_2CH_3\}_4]$ (**2**). In the absence of CuBr, only intractable mixtures were obtained. While the role of CuBr in the synthesis remains enigmatic, it is absolutely essential to the formation of **2**. The presence of the ligand in **2** was confirmed by the strong band observed at 1043 cm^{-1} in the infrared spectrum. The pattern of bands in the region characteristic of ν(V–O$_t$) indicated the presence of both V(IV) and V(V) sites. As shown in Table II, clusters which contain exclusively V(V) sites generally exhibit ν(V–O$_t$) bands in the 940–960-cm^{-1} range, while features in the 970–980-cm^{-1} region are characteristic of decavanadium clusters possessing exclusively V(IV) centers. The observation both of multiple bands in the 970–980-cm^{-1} range of a strong absorbance at 940–950 cm^{-1} appears to provide a useful diagnostic for the presence of a mixed-valence decavanadium core. As anticipated, compounds **3** and **4** exhibit a similar pattern of infrared bands in the 940–980-cm^{-1} region.

The synthesis of $K_2[V^{IV}{}_8V^V{}_2O_{16}\{(OCH_2)_3CCH_2CH_3\}_4]\cdot 2H_2O$ (**3**) also required the presence of a metal halide, in this instance $MnCl_2$. Once again, while necessary for the isolation of **3**, the role of $MnCl_2$ has not been determined.

(15) Haushalter, R. C.; Mundi, L. A. *Materials* **1992**, *4*, 31 and references therein.

(16) Lii, K. H.; Haushalter, R. C. *J. Solid State Chem.* **1987**, *69*, 320. Haushalter, R. C.; Lai, F. W. *J. Solid State Chem.* **1988**, *76*, 218. Haushalter, R. C. *J. Chem. Soc., Chem. Commun.* **1987**, 374. Haushalter, R. C.; Lai, F. W. *Angew. Chem.* **1989**, *101*, 802. Haushalter, R. C.; Lai, F. W. *Inorg. Chem.* **1989**, *28*, 2904. Haushalter, R. C.; Lai, F. W. *Science* **1989**, *246*, 1289. Corcoran, E. W. *Inorg. Chem.* **1990**, *29*, 157.

(17) Huan, G.; Day, V. W.; Jacobson, A. J.; Goshorn, D. P. *J. Am. Chem. Soc.* **1991**, *113*, 3188. Huan, G.; Greaney, M. A.; Jacobson, A. J. *J. Chem. Soc., Chem. Commun.* **1991**, 260. Huan, G.; Jacobson, A. J.; Day, V. W. *Angew. Chem., Int. Ed. Engl.* **1991**, *30*, 4.

(18) Lii, K. H.; Tsai, H. J. *J. Solid State Chem.* **1991**, *90*, 291. Lii, K. H.; Wang, Y. P.; Wang, S. L. *J. Solid State Chem.* **1989**, *80*, 127. Lii, K. H.; Tsai, H. J.; Wang, S. L. *J. Solid State Chem.* **1990**, *87*, 396. Lii, K. H.; Wang, S. L. *J. Solid State Chem.* **1989**, *82*, 239. Lii, K. H.; Wang, Y. P.; Chen, Y. B.; Wang, S. L. *J. Solid State Chem.* **1990**, *86*, 143 and references therein. Lii, K. H.; Li, C. H.; Chen, T. M.; Wang, S. L. *Z. Kristallogr.* **1991**, *197*, 67. Lii, K. H.; Lee, C. S. *Inorg. Chem.* **1990**, *29*, 3298. Wang, S. L.; Kang, H. Y.; Cheng, C. Y.; Lii, K. H. *Inorg. Chem.* **1991**, *30*, 3496. Lii, K. H.; Tsai, H. J. *Inorg. Chem.* **1991**, *30*, 446. Lii, K. H.; Tsai, H. J. *J. Solid State Chem.* **1991**, *91*, 331. Lii, K. H.; Wen, N. S.; Su, C. C.; Chen, B. R. *Inorg. Chem.* **1992**, *31*, 439.

Table III. Voltammetric Parameters for the Redox Processes of **4**[a]

compd[b]	$E_{1/2}$, V[c]	$E_p^f - E_p^r$, mV	i_p^f/i_p^r	$i_p/Cv^{1/2}$, mA $s^{1/2}$ $mV^{-1/2}$ M^{-1} [d]	n_{app}[e]
4	−0.012	65	1.0	9.1	1.0
	+0.363	72	1.0	9.2	1.0

[a] At a platinum-bead working electrode, using solutions 1.0×10^{-3} M in complex in 0.1 M $(Bu_4N)PF_6$ in acetonitrile or *N,N*-dimethylformamide. All potentials are referred to the ferrocene/ferrocenium couple. Cyclic voltammograms were obtained at sweep rates of 200 mV s^{-1}. [b] TBA = $(n\text{-}C_4H_9)_4N^+$. [c] Estimated from $E_{1/2} = (E_p^f - E_p^r/2 \sim E_p^f - 29$ mV. The shape parameter $E_p^f - E_p^r$ lay within the range 60–80 mV for all couples. [d] The current function for the ferrocene/ferrocenium couple at the same electrode is 9.2 mA $s^{1/2}$ $mV^{-1/2}$ M^{-1}. [e] The value of n (number of electrons) was determined by controlled-potential electrolysis at a potential 0.2 V from the process of interest.

The marked cation dependence of the hydrothermal syntheses of both hexavanadium and decavanadium clusters has been noted.[10,11] In the presence of ammonium cation as mineralizer, only the previously reported V(IV) decanuclear cluster $(NH_4)_4[V^{IV}_{10}O_{16}\{(OCH_2)_3CCH_2CH_3\}_4]\cdot H_2O$ (**5**) could be isolated, while quaternary salts R_4N^+ yielded a species with the cluster stoichiometry 5:10 $[CH_3CH_2C(CH_2O)_3]^{3-}$:V, namely $(Et_4N)[V_{10}O_{13}\{(OCH_2)_3CCH_2CH_3\}_5]$. In contrast, when Me_3NH^+, Na^+, and K^+ are used as mineralizers, both hexavanadium and decavanadium clusters may be isolated by appropriate modification of reaction conditions. Similar cation dependencies have been demonstrated in the molybdophosphate[16] and vanadophosphonate chemistries.[17]

Since compounds **1–3** and **5** are totally insoluble solids, considerable efforts were invested in attempts to prepare soluble examples of polyoxoalkoxides of the decavanadium core by introducing appropriate cations. After prolonged heating of a mixture of V_2O_5, $VO(SO_4)$, V_2O_3, $(HOCH_2)_3CCH_3$, and (TBA)OH in water in the molar ratio 3:3:6:10:10:110, dark brown blocks of $(TBA)_2[V_{10}O_{16}\{(OCH_2)_3CCH_3\}_4]$ (**4**) were isolated in 45% yield. In contrast to the synthesis of **2** and **3**, **4** did not require the presence of additional metal halide. The infrared spectrum of **4** was consistent with the presence of ligand and of the mixed-valence $\{V_{10}O_{28}\}$ core. Significantly, the introduction of the larger quaternary cation endowed this compound with good solubility in acetonitrile and dimethylformamide, providing a unique example of a member of the class of derivatized decavanadium clusters whose solution properties could be evaluated.

Given the existence of at least two cluster oxidation states $[V_{10}O_{16}\{(OCH_2)_3CR\}_4]^{4-}$ and $[V_{10}O_{16}\{(OCH_2)_3CR\}_4]^{2-}$ for this class of decavanadate coordination complex, the electrochemical behavior of **4** was of particular interest to us. The electrochemical characteristics of **4** are summarized in Table III, while Figure 1 shows the cyclic voltammogram of **4** in acetonitrile/(TBA)PF_6 solution. The electrochemical parameters are consistent with two successive reversible one-electron oxidations:

$$[V_{10}O_{16}\{(OCH_2)_3CH_3\}_4]^0 \overset{+0.36\text{ V}}{\underset{1e^-}{\rightleftharpoons}} [V_{10}O_{16}\{(OCH_2)_3CH_3\}_4]^- \overset{-0.01\text{ V}}{\underset{1e^-}{\rightleftharpoons}} [V_{10}O_{16}\{(OCH_2)_3CH_3\}_4]^{2-}$$

Controlled-potential electrolysis at +0.02 V resulted in a dramatic color change in the solution from the characteristic charcoal gray of **4** to deep green associated with $[V_{10}O_{16}\{(OCH_2)_3CH_3\}_4]^-$ (**4a**). Further electrolysis at +0.460 V of this latter solution results in a dark blue solution of the neutral $[V_{10}O_{16}\{(OCH_2)_3CH_3\}_4]$ (**4b**).

While "fully reduced" species of the type $[V_{10}O_{16}\{(OCH_2)_3CR\}_4]^{4-}$ may be produced in the hydrothermal synthesis, no reduction products of **4** are observed in the electrochemical window available in acetonitrile or CH_2Cl_2 solutions. However, addition of HBF_4 to solutions of **4** yielded the deep blue $[V_{10}O_{14}(OH)_2\{(OCH_2)_3CCH_3\}_4]^0$ (**4c**), whose cyclic voltammetry exhibits a quasi reversible one-electron reduction associated with

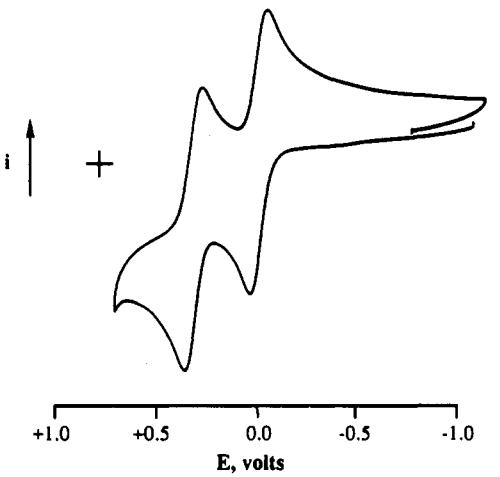

Figure 1. Cyclic voltammogram of **4**: 1.0×10^{-3} M in complex, 10^{-1} M (TBA)PF_6 in CH_3CN, Pt working electrode; ferrocene/ferrocenium reference.

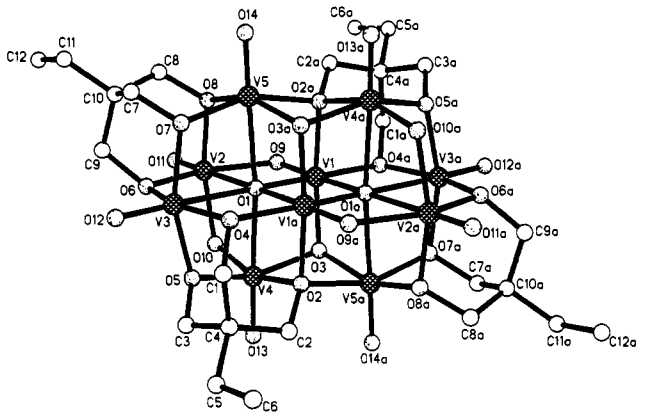

Figure 2. Schematic representation of the structures of the anions of **1–4**. A Pluto drawing is showing the atom-labeling scheme; for **1** C_6 and C_{12} are replaced by O_{15} and O_{16}, respectively, while for **4** the ligand alkyl chain terminates at C_5 and C_{11}.

the following electrochemical process:

$$[V_{10}O_{14}(OH)_2\{(OCH_2)_3CCH_3\}_4]^0 \overset{-0.10\text{ V}}{\rightleftharpoons} [V_{10}O_{14}(OH)_2\{(OCH_2)_3CCH_3\}_4]^-$$

Further details of the electrochemical and chemical properties of **4** and related soluble decavanadate coordination complexes are under investigation.

Structural Features. As shown in Figure 2, the structures of the anions of **1–4** possess the gross metal–oxygen framework of the $[V_{10}O_{28}]^{6-}$ and $[H_nO_{10}O_{28}]^{(6-n)-}$ ($n = 2, 3$) prototypes.[19-21] In the structures of this study, ten doubly bridging oxo groups and two triply bridging oxo groups of the parent $\{V_{10}O_{28}\}$ core have been replaced by twelve alkoxy donors from the four trisalkoxy ligands. As noted previously for the structure of $(NH_4)_4[V_{10}O_{16}\{(OCH_2)_3CCH_2CH_3\}_4]\cdot 4H_2O$ (**5**),[13] the pattern of substitution adopted by the trisalkoxy ligands in these structures is dictated by the bonding requirements of the ligands which will bridge between three metals in a triangulo arrangement when possible, giving the ligands a strong tendency to cap the triangular faces of the tetrahedral cavities of the decametalate framework. As shown in Figure 3, there are six potential sites for the trisalkoxy ligands, of which four are occupied in the structures of this study and also in **5**.

There are notable differences between the structures of this study and that previously reported for **5**. Variably protonated

(19) Fuchs, J.; Mahjour, S.; Palm, R. *Z. Naturforsch.* **1976**, *31b*, 544.
(20) Corigliano, F.; DiPasquale, S. *Inorg. Chim. Acta* **1975**, *12*, 99.
(21) Evans, H. T.; Pope, M. T. *Inorg. Chem.* **1984**, *23*, 501.

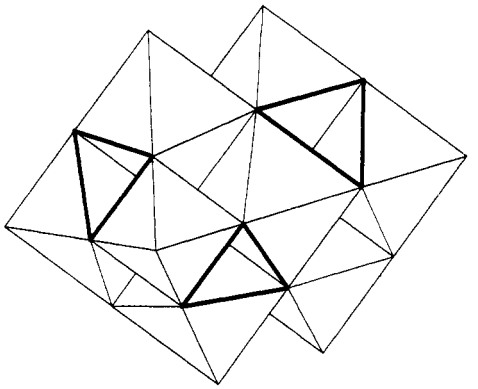

Figure 3. Schematic representation of the $\{V_{10}O_{28}\}$ core. The triangular faces available for occupation by trisalkoxy oxygen donors are highlighted.

Table IV. Selected Bond Lengths (Å) for the Structures of $(Me_3NH)_2[V_{10}O_{14}(OH)_2\{(OCH_2)_3CCH_2OH\}_4]\cdot 2H_2O$ (**1**), $Na_2[V_{10}O_{16}\{(OCH_2)_3CCH_2CH_3\}_4]$ (**2**), $K_2[V_{10}O_{16}\{(OCH_2)_3CCH_2CH_3\}_4]_2\cdot 2H_2O$ (**3**), $[(n\text{-}C_4H_9)_4N]_2V_{10}O_{16}\{(OCH_2)_3CCH_3\}_4]$ (**4**), and $(NH_4)_4[V_{10}O_{16}\{(OCH_2)_3CCH_2CH_3\}_4]\cdot 4H_2O$ (**5**)

	1	2	3	4	5
V1–O1	2.008(3)	2.007(4)	2.007(4)	2.012(4)	2.014(3)
V1–O1a	2.147(3)	2.148(4)	2.122(3)	2.140(4)	2.140(3)
V1–O2	2.086(3)	2.057(4)	2.063(2)	2.070(4)	2.077(3)
V1–O3	1.929(3)	1.945(4)	1.926(2)	1.935(4)	1.935(3)
V1–O4	1.964(3)	1.975(3)	1.975(2)	1.970(4)	1.968(3)
V1–O9	1.669(3)	1.665(4)	1.678(3)	1.663(4)	1.656(3)
V2–O1	2.441(3)	2.449(4)	2.456(3)	2.337(4)	2.447(3)
V2–O6	1.988(3)	1.981(4)	1.984(2)	1.999(5)	1.994(3)
V2–O8	2.001(3)	2.010(4)	2.000(2)	2.008(4)	1.995(3)
V2–O9	2.026(3)	2.017(4)	2.020(2)	2.026(4)	2.017(3)
V2–O10	1.996(3)	1.999(4)	1.979(2)	1.960(4)	1.971(4)
V2–O11	1.596(3)	1.584(4)	1.591(3)	1.591(5)	1.586(3)
V3–O1	2.366(3)	2.296(4)	2.350(2)	2.337(4)	2.322(3)
V3–O4	2.019(3)	2.025(4)	2.034(3)	2.020(4)	2.012(3)
V3–O5	2.013(3)	2.000(4)	2.004(2)	2.023(4)	2.004(3)
V3–O6	2.011(3)	1.983(4)	1.996(3)	2.008(5)	2.000(3)
V3–O7	2.008(3)	2.020(4)	2.020(4)	1.997(4)	1.997(3)
V3–O12	1.595(3)	1.599(4)	1.599(2)	1.586(5)	1.599(3)
V4–O1	2.407(3)	2.375(4)	2.400(2)	2.415(4)	2.407(3)
V4–O2	2.088(3)	2.202(4)	2.190(3)	2.202(4)	2.135(3)
V4–O3	1.978(3)	1.923(4)	1.932(2)	1.908(4)	1.933(3)
V4–O5	1.980(3)	1.951(4)	1.947(2)	1.972(5)	1.966(3)
V4–O10	1.943(4)	1.722(4)	1.711(3)	1.695(4)	1.813(3)
V4–O13	1.596(3)	1.601(4)	1.598(2)	1.601(5)	1.589(4)
V5–O1	2.367(3)	2.378(4)	2.324(2)	2.313(4)	2.351(3)
V5–O2	2.084(3)	2.044(4)	2.002(2)	2.054(4)	2.068(3)
V5–O3	1.994(3)	1.994(4)	1.984(2)	1.987(4)	1.981(3)
V5–O7	1.985(3)	2.007(4)	2.002(2)	1.991(5)	1.991(3)
V5–O8	2.002(3)	1.996(4)	2.005(3)	2.013(4)	2.007(3)
V5–O14	1.596(3)	1.593(4)	1.604(2)	1.595(5)	1.587(4)

forms of oxidized polyoxovanadate clusters are well-established, for example $[H_nV_{10}O_{28}]^{(6-n)-}$ (n = 0, 2, and 3)[21-23] and $[H_nPV_{14}O_{42}]^{(9-n)-}$.[24,25] Compound **1** represents a relatively unusual example of structurally characterized reduced core exhibiting bridging hydroxy groups. Valence sum calculations[26] for each of the vanadium centers of **1** and **5** based on the data of Table III confirm that all metal centers are in the "reduced" +4 oxidation state. However, the crystallographic study establishes O10 and O10a as the protonation sites, a feature consistent both with the location of the excursions of electron density in the difference Fourier maps and with the V–O10 distances tabulated in Table IV. The significant lengthening of the V–O10 bond distance in **1** compared to that observed for **5** is consistent with protonation of this site. We have noted in the study of the structures of the hexavanadate series of complexes $[V_6O_{13-n}(OH)_n\{(OCH_2)_3CR\}_2]^{2-}$ (n = 0, 4, 6)[10] that V(IV)–doubly bridging hydroxy distances are in the order of 1.95 Å as compared to a value of 1.87 Å for V(IV)–doubly bridging oxo-group distances. It has been established for oxidized polyvanadates of the types $[H_nV_{10}O_{28}]^{(6-n)-}$ [21-23] and $[H_nPV_{14}O_{42}]^{(9-n)-}$ [24,25] that doubly- and triply-bridging oxo groups provide the protonation sites as a consequence of the greater basicity of these in relation to terminal oxo groups, a feature recently confirmed by ab initio SCF calculations.[27] It is significant that in the structure of $[H_2V_{10}O_{28}]^{4-}$ [22] it is the symmetrically doubly-bridging oxo groups connecting vanadium sites of the central $\{V_6O_{12}\}$ girdle with the "apical" vanadium centers, such as V4 and V5 of this study, which are protonated in preference to the oxo groups which bridge two adjacent vanadium sites within the equatorial girdle. This latter type of doubly-bridging oxo group adopts an unsymmetrical bridging mode, with significant multiple bond character in the interaction with the central vanadium centers of the $\{V_6O_{12}\}$ core and concomitantly weaker bonding to the peripheral vanadium sites. Consequently, the doubly-bridging oxo groups of type O9 possess characteristics of terminal oxo groups (V1–O9 = 1.670(3) Å) and would not be expected to protonate as readily as a conventionally bridging oxo group. While both doubly- and triply-bridging oxo groups of $[H_3V_{10}O_{28}]^{3-}$ [23] are protonated, the protonated doubly-bridging sites are those spanning the equatorial vanadium and apical vanadium centers, in similar fashion to $[H_2V_{10}O_{28}]^{4-}$ and **1**.

The structures of the anions of **2–4** are essentially identical but exhibit significant departures from those observed for the anions of both **1** and **5**. As shown in Table IV, the most significant difference in the bond lengths is associated with V4–O10, which is 1.72 Å (average) for **2–4** as compared to 1.943(3) Å for **1** and 1.813(3) Å for **5**. Such significant bond length contraction suggests that V4 is present in the +5 oxidation state and that **2–4** are mixed-valence complexes containing the $[V^{IV}_8V^{V}_2O_{16}\{(OCH_2)_3CR\}_4]^{2-}$ anion. Valence sum calculations based on the bond length data of Table IV are consistent with the +5 oxidation state for V5 (V5a) and +4 for all other vanadium centers of **2–4**. The distinguishable geometries of the vanadium centers of **2–4** establish these species as class I mixed-valence clusters[28] where the d^0 sites are localized on V5 and V5a.

The structural features associated with the anions of **2–4** serve to rationalize the observed infrared spectra of these species. As previously noted, the unique feature of these spectra is the presence of multiple band patterns in the 940–980-cm^{-1} range, which are absent from the spectra of the mixed-valence clusters of the hexavanadium class. This complexity of the spectra reflects the variety of V–O multiply bonded sites and, consequently, the different bond strengths associated with ν(V=O) in the $[V^{IV}_8V^{V}_2O_{16}\{(OCH_2)_3CR\}_4]^{2-}$ species. The distinct V=O types include conventional V(IV)–O(terminal) moieties for V2–O11, V3–O12, and V5–O14, a V(V)–O(terminal) unit for V4–O13, and the unsymmetrically bridging V(IV)–O and V(V)–O types, V1–O9, and V4–O10, respectively.

The compounds of this study, with the exception of **4**, are refractory solids and, as such, exhibit three-dimensional arrays reminiscent of nonmolecular materials. The structure of the species $(NH_4)_4[V_{10}O_{16}\{(OCH_2)_3CCH_2CH_3\}_4]\cdot 4H_2O$ (**5**) is prototypical of the extended frameworks adopted by this class of compounds. As shown in Figure 4a, there is extensive hydrogen bonding between the NH_4^+ cations and pairs of adjacent decavanadium anions. The overall pattern of hydrogen bonding is somewhat more complicated as the N1 site enjoys additional interactions to a decavanadium unit below the plane of Figure 4a, while the N2 cation is associated with an anion cluster above

(22) Capparelli, M. V.; Goodgame, D. M. L.; Hayman, P. B.; Skapski, A. C. *J. Chem. Soc., Chem. Commun.* **1986**, 776.
(23) Day, V. W.; Klemperer, W. G.; Maltbie, D. J. *J. Am. Chem. Soc.* **1987**, *109*, 2991.
(24) Kato, R.; Kobayaski, A.; Sasaki, Y. *Inorg. Chem.* **1982**, *21*, 140.
(25) Khan, M. I.; Zubieta, J.; Toscano, P. *Inorg. Chim. Acta* **1992**, *193*, 17.
(26) Brown, I. D.; Altermatt, D. *Acta Crystallogr.* **1985**, *B41*, 244.
(27) Kempf, J.-Y.; DeRohmer, M.-M.; Poblet, J.-M.; Bo, C.; Bénard, M. *J. Am. Chem. Soc.* **1992**, *114*, 1136.
(28) Robin, M. D.; Day, P. *Adv. Inorg. Chem. Radiochem.* **1967**, *10*, 247.

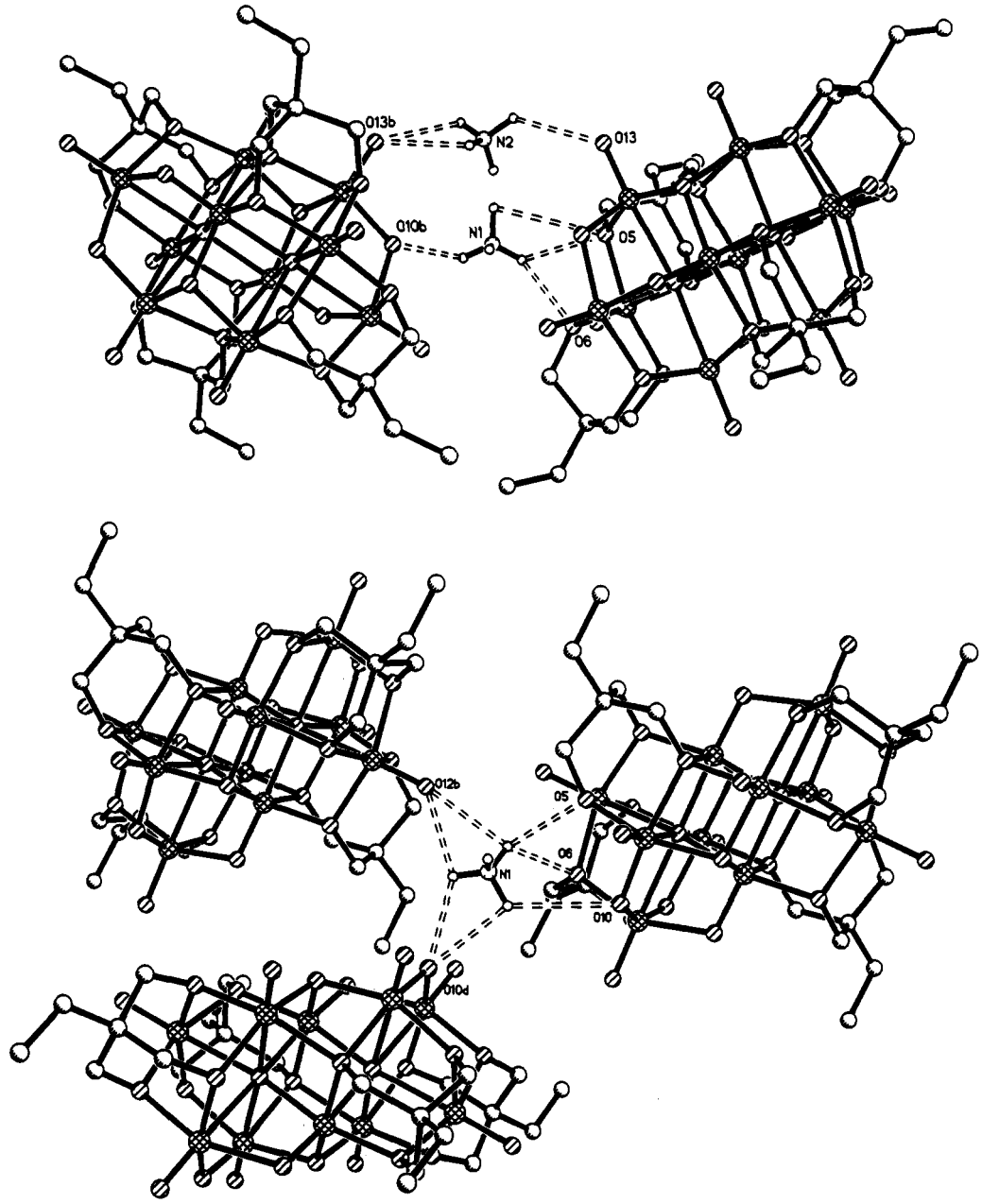

Figure 4. (a) Top: View of the hydrogen bonding between two anion clusters and the interleaved NH_4^+ cations in **5**. (b) Bottom: Environment of the N1 ammonium cation site in **5**.

this plane. Figure 4b illustrates the overall pattern of hydrogen bonding for the N1 cation site. When the structure of **5** is viewed down the crystallographic *a* axis, the tunnel-like nature of the solid is revealed. The anions stack along the *a* direction to produce columns, while the cations occupy the cavities produced between these stacks. A significant feature of the stacking is that polar and nonpolar regions are clearly segregated. Thus, the stacking of the anion clusters directs the hydrophobic alkyl substituents of four neighboring stacks toward a common channel. Similarly the polar V–O groups form the "walls" of the channels which encapsulate the cations. Compound **5** is thus amphiphilic, and the crystal packing of the compounds of this class can be rationalized on the basis of such hydrophobic–hydrophilic interactions.

Figure 5 illustrates the interactions of the Na^+ cation of **2** with adjacent decavanadium anion clusters. Significantly, there are strong interactions between Na^+ and O13 and O10, which are bonded to V4, the oxidized site of the cluster. A similarly strong interaction is found in **3** between K^+ and these sites. This observation suggests that the V(V) site found in the anion clusters of **2** and **3** is stabilized by the proximity of the electropositive alkali metal cation. The oxide ions in **2** form a nearly close-packed array with the cations firmly held within the interstices formed between the anion clusters.

The extended structure of **2** consists of the common tunnel array, with the cavities aligned along the short crystallographic *b* axis. In the comparison of this extended structure with that of **5**, the dramatic influence of the cation in determining the three-dimensional packing is apparent. Once again, the segregation of polar and nonpolar region is observed, but in this instance, the alignment of the alkyl substituents produces hydrophobic planes parallel to the crystallographic *bc* planes. The Na^+ cations occupy the polar channels between the anion stacks.

The three-dimensional structure of the K^+ derivative **3** is yet again different in detail. Figure 6a shows the interactions between the K^+ cations and neighboring anion clusters. Pairs of potassium cations are bridged by H_2O molecules in $[K_2(H_2O)_2]^{2+}$ units which are sandwiched between neighboring pairs of cluster anions. These units interact through additional K–O contacts to produce a one-dimensional polymeric chain. Comparison with Figure 6a with Figure 5 clearly illustrates the structural reorganization accompanying cation substitution. However, it is significant that O10 and O13, both bonded to the V(V) site V4, form close contacts with the cation in structure **3**, as well as that of **2**.

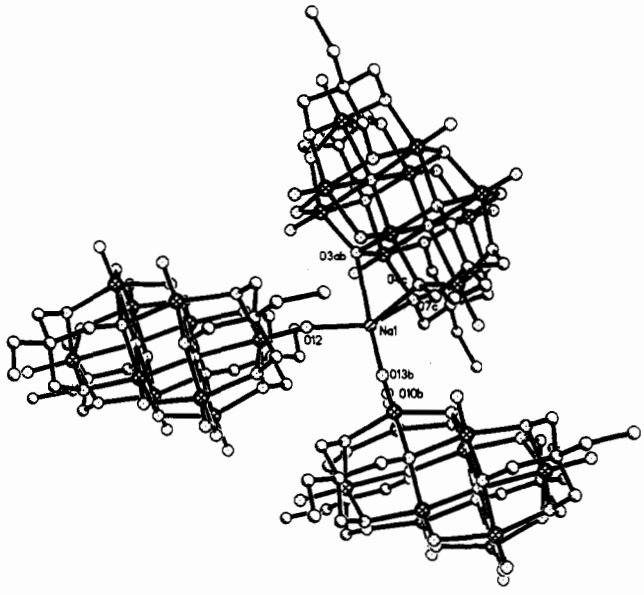

Figure 5. Na^+ cation environment in **2**.

A view of the crystal packing of **3** along the short crystallographic *c* axis illustrates that the common motif of anion stacking is again adopted. The polar and nonpolar regions are differentiated as in **2** and **5**, and the cations and the water molecules are observed to occupy the polar channels.

The extended structure of **1** presents some unique features, as might be anticipated from the presence of the Me_3NH^+ cations. Figure 7a illustrates the hydrogen bonding adopted between pairs of cluster anions and the water molecules of crystallization. The hydrogen atoms of the bridging OH groups of the anion clusters participate in hydrogen bonding to neighboring anion clusters, as well as the hydrogen atoms of the water molecules interleaved between pairs of clusters, producing a polymeric chain $\{[V_{10}O_{14}(OH)_2\{(OCH_2)_3CCH_2OH\}_4]^{2-}\cdot H_2O\}_\infty$. The Me_3NH^+ cation is also strongly hydrogen bonded through the interaction of H1 and O3, shown in Figure 7b. In the perspective of Figure 7a, the cations occupy positions above and below the anion clusters, rather than in the intercluster channel. The stacking motif common to this structural type is retained. However, the cations do not occupy the channels but are partially obscured from this perspective by the anion stacks. As shown in Figure 7c, rather than occupying channels between anion stacks, the Me_3NH^+ cations are slotted into the walls of the cluster stacks and project into the nonpolar regions between anion columns. This view of the packing also shows that polar and nonpolar channels are not as clearly delineated in **1** as in the structures of **2**, **3**, and **5**.

The crystal packing pattern exhibited by **4** contrasts with that of **1** and with that adopted by $[(C_2H_5)_4N][V_{10}O_{13}\{(OCH_2)_3CCH_2CH_3\}_5]$ (**6**), where the presence of a tetraorganoammonium cation also appears to dictate the orientational relationship of anions and cations in the solid. Figure 8a illustrates the environment of the $(C_2H_5)_4N^+$ cation (TEA) in **6** and the hydrophobic nature of the pockets occupied by the cations. The cations of **6** are again displaced from the channels between anion stacks and slotted into the crevices between adjacent cluster columns. Isolation of two pairs of adjacent stacks ligands in Figure 8b presents a clear view of the cation stacking pattern. The solid-state structures adopted by **1** and **6** appear to reflect a compromise between most efficient packing in the crystal and the presence of large organic cations which would serve to increase the interstack channel volume were they to occupy discrete interleaved stacks, as do the inorganic cations of **2**, **3**, and **5**.

The solubility properties of $(TBA)_2[V_{10}O_{16}\{(OCH_2)_3CCH_3\}_4]$ (**4**) would suggest a departure from the extended structural motifs adopted by **1** and **6**. Figure 9 illustrates the environment of a single anion cluster, which is surrounded by six quaternary

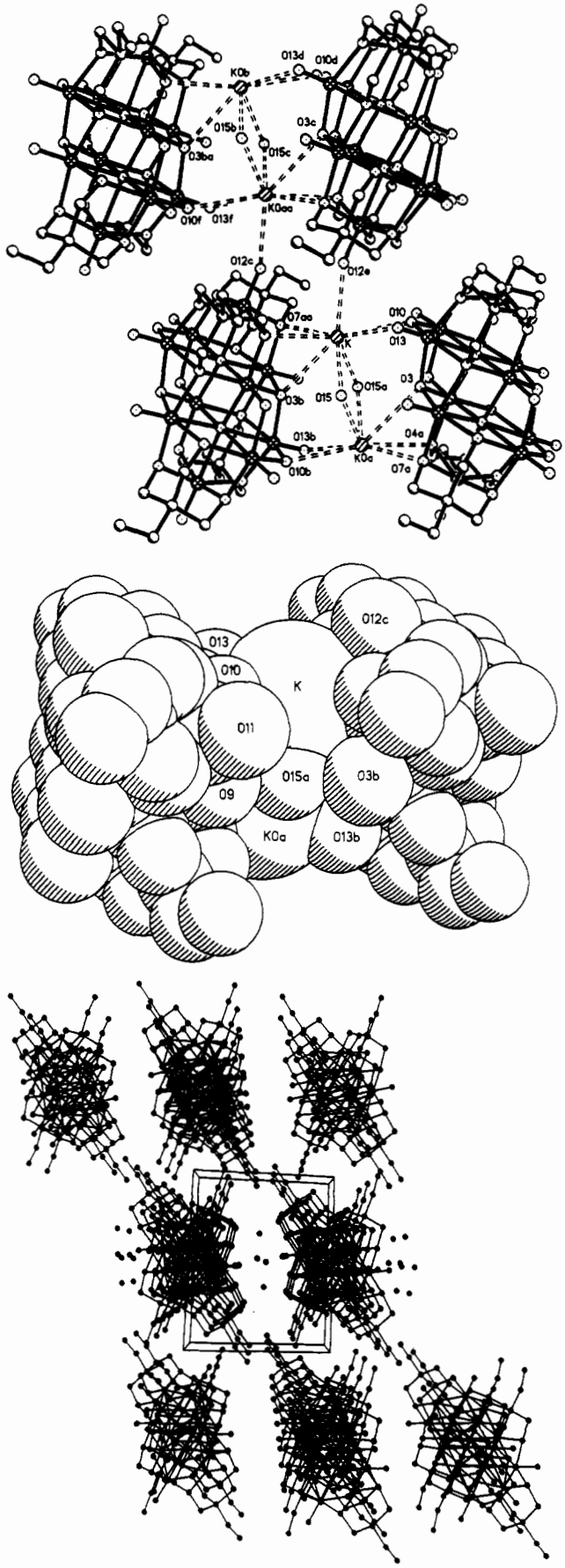

Figure 6. (a) Top: K^+ cation environment in **3**, showing the geometry of the binuclear $[K_2(H_2O)_2]^{2+}$ units. (b) Middle: Space-filling view of the $[K_2(H_2O)_2]^{2+}$ environment, showing the sandwiching of this unit between two clusters. (c) Bottom: View of the crystal packing viewed along the crystallographic *c*-axis of **3**, showing the occupancy of polar channels by the K^+ and H_2O.

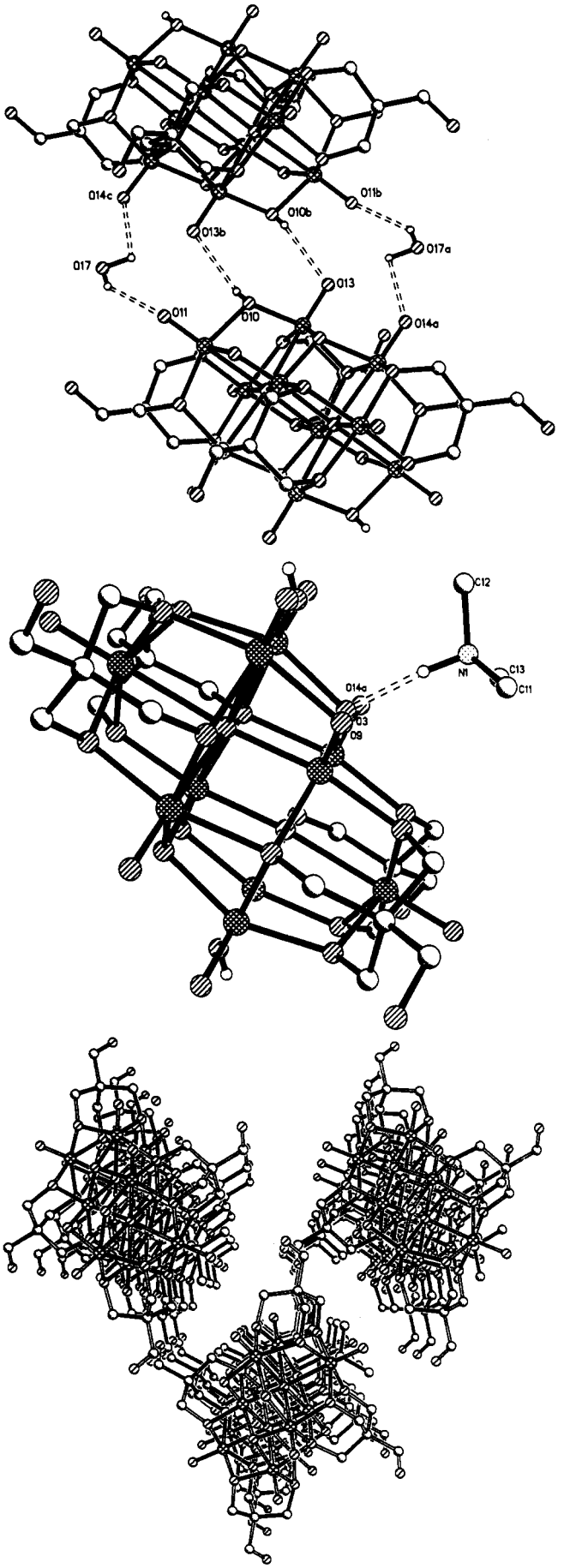

Figure 7. (a) Top: View of the hydrogen bonding between pairs of cluster anions and H_2O molecules of crystallization of **1**. (b) Middle: Environment of the Me_3NH^+ cation, showing the hydrogen-bonding interaction between H and O3. (c) Bottom: Perspective view of the stacking in **1** with the cations highlighted.

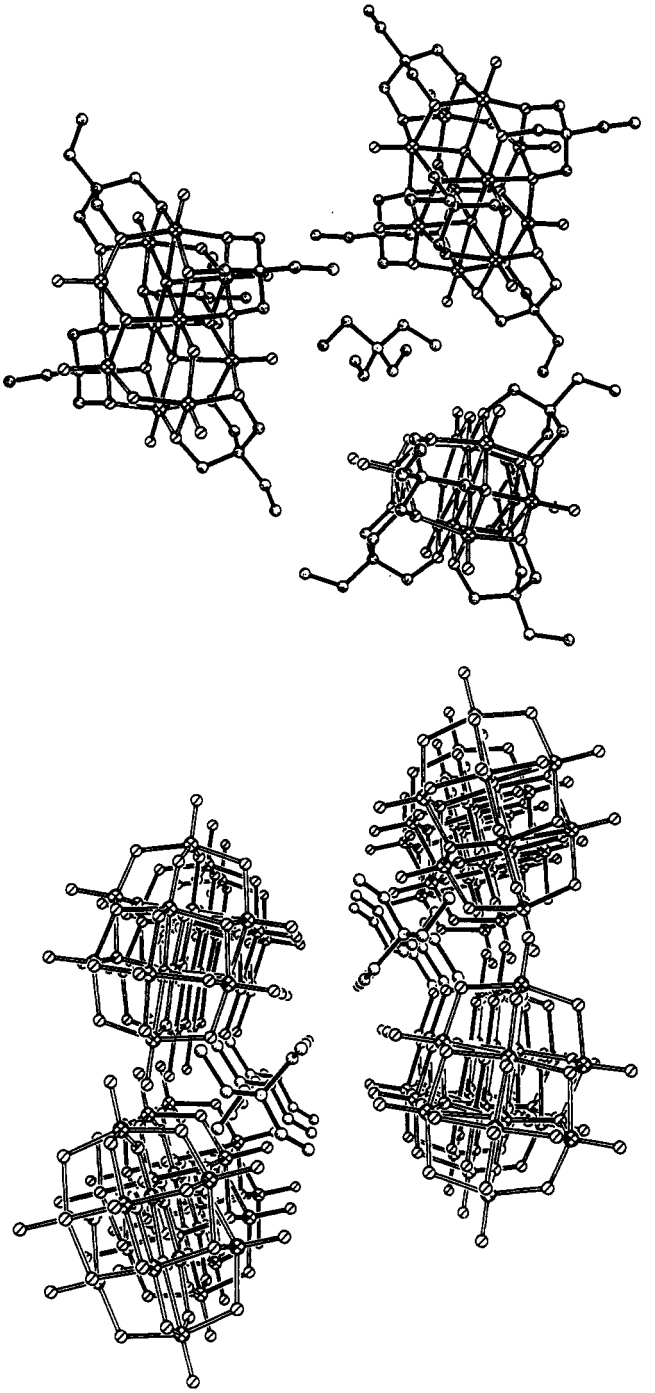

Figure 8. (a) Top: Environment of the $(C_2H_5)_4N^+$ cation in **6**. (b) Bottom: Depth-queued view of the cation and anion stacking with ligand carbons removed for clarity.

ammonium cations in a hydrophobic pocket. The organic cations are now segregated from the anion stacks in well-defined channels. The introduction of the large organic cations, as anticipated, decreases the packing efficiency, effectively reducing the density of the crystals and enhancing solubility.

While the other examples of derivatized decavanadium clusters with organic cations, **1** and **6**, exhibit exclusively V(IV) sites, **4** is a mixed-valence species, similar to **2** and **3**. While the structures of **2** and **3** clearly reveal the role of the cation in stabilizing the V(V) sites, this is not the case in **4**. The presence of oxidized sites in **4** may thus reflect the need to achieve charge balance while maintaining a degree of efficiency in crystal packing. It may be relevant to this argument that the parent anion $[V_{10}O_{28}]^{6-}$ does not provide a crystalline material with TBA cation but in the presence of a smaller dipositive cation $(H_3NCH_2CH_2NH_3)^{2+}$ does yield crystalline $(H_3NCH_2CH_2NH_3)_3[V_{10}O_{28}]\cdot 6H_2O$.[29]

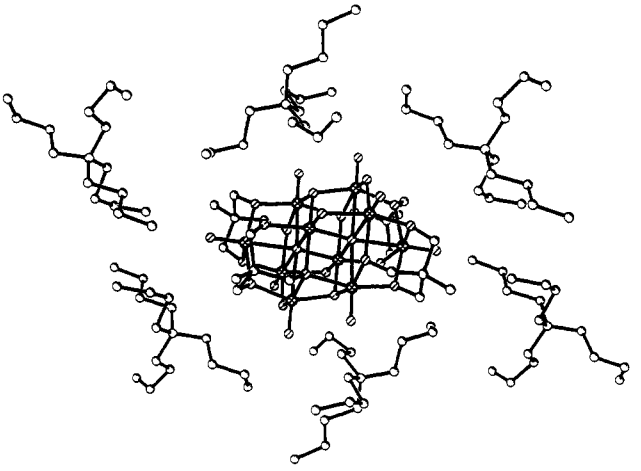

Figure 9. Anion environment of **4**.

Similarly, $[H_2V_{10}O_{28}]^{4-}$ will crystallize only in the presence of less sterically demanding organic cations.[22,29,30]

Magnetic Susceptibility Studies. Variable-temperature solid-state magnetic susceptibility studies were performed on powdered samples of **1–3** in the range 4.2–300 K. Figures 10 and 11 show plots of the gram susceptibility (χ) and effective moment (μ_{eff}) per molecule.[31] The theoretical spin only moment in the absence of coupling for a ten V(IV)-d^1 system is 5.47 μ_B/molecule. The effective magnetic moment of **1** at 300 K is 4.45 μ_B/molecule, indicating net antiferromagnetic exchange coupling and corresponding to 1.41 μ_B/V(IV) center. The data are distinctly nonlinear, particularly below 100 K. At higher temperature, the data approach Curie–Weiss behavior, with a paramagnetic Curie temperature $\Theta = -160$ K. The effective moment of **1** decreases with temperature to 1.96 μ_B at 5 K (0.63 μ_B/V(IV) center).

The effective moment of **2** at 300 K is 4.24 μ_B/molecule (1.50 μ_B/V(IV) site), again indicative of antiferromagnetic coupling; the theoretical spin only moment in the absence of coupling for an eight V(IV)-d^1 system is 4.89 μ_B/molecule. At high temperatures, the data approach Curie–Weiss behavior with $\Theta = -132$ K. The magnetic susceptibility of **2** increases with decreasing temperature, reaching a maximum at Néel temperature of 23 K, indicating strong antiferromagnetic ordering.

The results are similar to those previously reported for **5**[13] and to those observed by Müller et al.[32] for a number of V(IV)-containing clusters. While species with small numbers of V(IV) sites, compared to the total number of vanadium centers, exhibit trapped and separated d^1 centers and consequently spin only values for μ_{eff}/μ_B per V(IV), spin–spin coupling increases with increasing numbers of V(IV) centers, producing decreased values of μ_{eff}/μ_B.

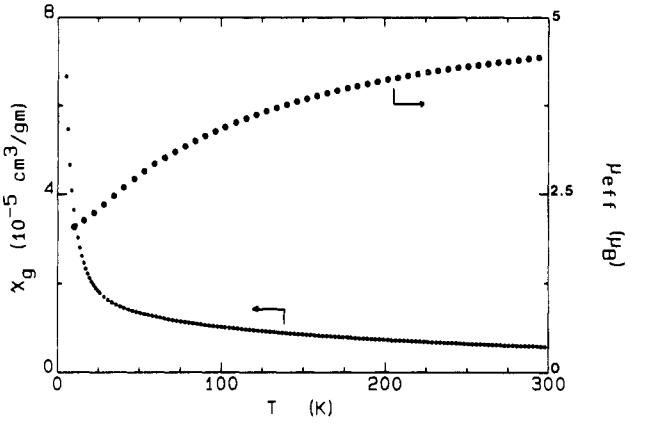

Figure 10. Plot of the magnetic susceptibility (χ_g) and effective moment (μ_{eff}) per molecule for **1**.

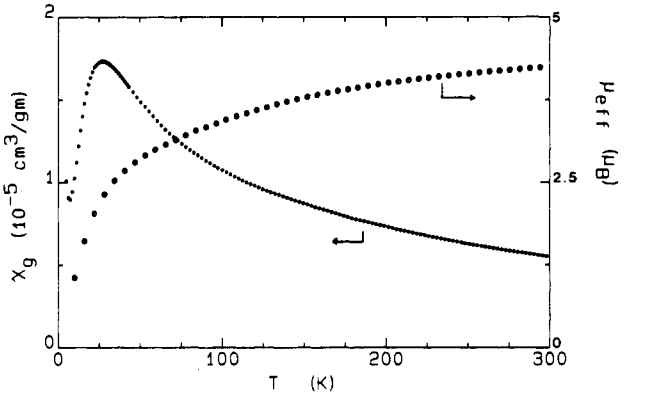

Figure 11. Plot of the magnetic susceptibility (χ_g) and effective moment (μ_{eff}) per molecule for **2**.

Acknowledgment. This work was supported by a grant from the National Science Foundation (CHE9119910).

Supplementary Material Available: Tables listing crystal data and experimental conditions for the X-ray studies of **1–4**, atomic positional parameters, bond lengths, bond angles, and anisotropic temperature factors and figures showing crystal packing and space-filling views of structures **1–6** (57 pages). Ordering information is given on any current masthead page.

(29) Shao, M.; Wang, L.; Zhang, Z.; Tang, Y. *Sci. Sin., Ser. B (Engl. Ed.)* **1984**, *27*, 137 and references therein.
(30) Debeardemacher, T.; Arrieta, J. M.; Amigo, J. M. *Acta Crystallogr.* **1982**, *B32*, 2465.
(31) Carlin, R. L. *Magnetochemistry*; Springer-Verlag: Berlin, 1986.
(32) Müller, A.; Döring, J.; Bögge, H. *J. Chem. Soc., Chem. Commun.* **1991**, 273 and references therein.